# Real-time Prediction of Key Monitoring Physical Parameters for Early Warning of Fire-induced Building Collapse

Wei Ji[1], Guo-Qiang Li[1,2], Shaojun Zhu[1*]

[1] College of Civil Engineering, Tongji University, Shanghai 200092, China

[2] State Key Laboratory of Disaster Reduction in Civil Engineering, Tongji University, Shanghai 200092, China

[*] Corresponding author E-mail: zhushaojun@tongji.edu.cn



**Abstract**

This paper proposes a real-time prediction method for key monitoring physical parameters (KMPPs) for early warning of fire-induced building collapse using machine learning. Since the actual load distribution and structural material properties of the burning building are usually unknown and uncertain, easy-to-measure parameters of the burning building, including easy-to-measure KMPPs (displacements and displacement velocities) of key joints, and temperatures of key structural members of the building, are incorporated as the input to predict the hard-to-measure KMPPs. The long short-term memory network is adopted in the machine learning framework. The network can be trained offline during the design stage through simulated data and used online with real-time measured data in fire. A portal frame building is numerically examined, and the results indicate that the trained agent can identify unknown and uncertain parameters and predict the hard-to-measure KMPPs with high accuracy and efficiency, enhancing the accuracy and reliability of early warning for fire-induced building collapse.

**Keywords**

early warning of fire-induced collapse, real-time monitoring, key monitoring physical parameters, machine learning

## 1 Introduction

Fire safety is an important issue in structural design since an uncontrolled building fire may cause severe property losses and fatalities [1, 2]. As a result, current studies on structural fire engineering mainly focused on ensuring the safety of residents under fire conditions, and much progress has been achieved either in the aspects of improving the structural fire resistance [3−5] or suggesting fire evacuation strategies [6−8]. Recently, as the fire-induced building collapse has been a major threat to the safety of firefighters, as shown in Fig. 1, early warning of the building collapse is proposed to be a more and more important issue for firefighters [9, 10]. Previously, commanders at the fire rescue site could only make visual observations of the state of the burning building and make decisions based on their experiences, which is usually inaccurate and unreliable. Therefore, it is necessary to develop a scientific and reasonable method to raise on-site early warning of the fire-induced collapse in order to facilitate wise decisions on the evacuation of firefighters at the most appropriate time, which may greatly enhance the efficiency of the firefighters' rescue.

Fig. 1 Fire-induced collapse of a steel building. (a) Building before collapse. (b) Building after collapse

One essential issue in the real-time evaluation, or early warning of the collapse state of the structure for a burning building, is exploring the key monitoring physical parameters (KMPPs), which should meet the following requirements:

- R1 The KMPPs should have a specific and quantitative relationship with the ultimate collapse state;
- R2 The KMPPs should, at least, implicitly contain the information of uncertain parameters, e.g., the actual load distribution and intensity, structural material properties, and fire scenario;
- R3 The KMPPs should be easy to obtain under fire conditions.

In this way, although dynamic responses and natural frequencies of the structure will change under fire conditions due to stiffness degradation, their variation laws are hard to be summarized, and it is difficult to obtain them timely in real fire conditions, i.e., the parameters only satisfy requirement R2. In standard fire tests, the temperature, displacement, and displacement velocity are key parameters to evaluate the fire resistance of specimens [11]. Similarly, the collapse state of burning structures is proposed to be traced by monitoring the displacements and displacement velocities of key positions on the periphery of the structure [12–14], as they are proved to satisfy requirements R1 and R2. However, the high temperature and dense smoke in fire greatly influence the accuracy of contact displacement measurement systems and optical displacement measurement systems. Though microwave radars can overcome the difficulties mentioned above, it is still hard to directly measure the displacement of the joints at the top of the structure since the radars should be placed on the ground. Therefore, it is essential to develop a method for obtaining the hard-to-measure KMPPs, i.e., the displacements, in order to perfect the early warning method and theory of structural fire-induced collapses.

Here we notice that the temperature of key members can be easily acquired through pre-embedded thermocouples during the construction process. Besides, the structural response of a specific structure under a determinate fire scenario is determinate. Specifically, given specific load conditions and material properties, the displacements of the burning structure under a specific fire scenario, i.e., structural temperature field, can be uniquely determined. Traditional methods for this process include the thermal-structural coupling analysis using the finite element (FE) method. Roy *et al*. [15] established an FE model using ABAQUS to simulate the collapse behavior of a steel building in the fire test, and a deformed shape similar to the test result was acquired. Lausova *et al*. [16] adopted SCIA Engineer to study the deformation of a heated portal frame. Foster *et al*. [17] used VULCAN to model the structural response of the burning building in the Cardington test, and a satisfactory simulation result was obtained compared to the test data. Jiang *et al*. [18] studied the axial displacements of heated columns and vertical displacements of heated slabs in the fire-induced collapse process of a multi-story steel frame using LS-DYNA. Besides, OpenSees, a software initially designed for seismic analysis, was also extended to include the modeling of structures under fire load due to its open-source nature and object-oriented design, see Jiang *et al*. [19]. However, the thermal-structural coupling analysis is computationally expensive and time-consuming; hence, it is almost impossible to be conducted at fire rescue scenes for early warning of fire-induced collapse.

Some researchers proposed alternatives to thermal-structural coupling analysis for the mapping from measured temperature to the early-warning level [20] or the structural response [21]. However, we emphasize that the above methods are based on an unrealistic assumption, i.e., the material properties and the load distributions are assumed to be deterministic values in the design phase. In other words, the temperature cannot be considered as the only KMPP since it does not fully satisfy requirement R2. In addition, the uncertain structural parameters mentioned above are very hard to be explicitly identified in time at the fire rescue scene since the number of them almost equals the number of members. Notably, the early-warning theory for fire-induced collapse proposed by Li *et al*. [13, 14, 22] also introduced the reliability theory in order to consider the influence of various determinate structural geometric parameters, e.g., the span and height, on the early-warning level. In this way, failure to consider the uncertain structural parameters will cause higher errors, and the significance of early warning will decrease. Therefore, the temperature must be incorporated with other physical parameters in order to form KMPPs for early warning of fire-induced collapse.

With the development of the computer science, machine learning (ML) techniques have gained great popularity in the field of structural fire engineering to reduce the computational cost. Naser *et al*. [23] compared the performance of several ML algorithms in six structural and fire engineering problems using various performance metrics. Fang *et al*. [24] adopted an ML approach to identify the stages of the fire development in typical residential room fires using thermocouples. A satisfactory accuracy of 85% within 2 min error range was achieved compared with the experimental data. Mashhadimoslem *et al*. [25] used a multi-layer neural network to predict the flame lengths and width of a jet fire, and a good agreement with experimental results was achieved. Wang *et al*. [26] used the convolutional neural networks and smoke images to identify the transient fire heat release rate of the building fire, and the error was no more than 20%. Kou *et al*. [27] proposed a real-time estimation method of building fire location and intensity based on the gated recurrent unit. The reliability and efficiency of the method were studied through fire simulations. Besides, the physics-informed neural networks proposed by Raissi *et al*. [28] can effectively resolve complex and computationally expensive problems by introducing the residual of partial differential equations as physical constraints. As Samaniego *et al*. [29] and Rao *et al*. [30] used the physics-informed ML approach to solve linear elasticity and hyperelasticity problems in continuum mechanics and simulate incompressible laminar flows, its application in the field of fire dynamics is promising.

Recently, the recurrent neural network (RNN), which can rapidly deal with the non-linear mapping relationship of time series data, has achieved satisfying results in time-dependent structural response modeling [31]. Noteworthy, the long short-term memory (LSTM) network, an improved form of RNN, can solve the gradients vanishing and exploding problems of the traditional RNN, which makes it behave well in resolving long time series problems. Zhu *et al*. [32] adopted the LSTM network to predict the deterioration process of metro shield tunnels, and a better prediction over the traditional multi-layer neural networks was achieved. Zhang *et al*. [33] used the LSTM network to model the structural seismic response, and satisfactory results were obtained with respect to both synthetic data and field sensing measurements. Xu *et al*. [34] extended research [33] by introducing a recursive mechanism in the network architecture to improve the performance of time series prediction of seismic problems. As for applications in structural fire engineering, Zhang *et al*. [35] proposed a framework to forecast the fire development and flashover of compartment fires based on the LSTM network and temperature data. Analyses revealed that the trained model could adapt to various fuel types and ventilation conditions. Wu *et al*. [36] combined the LSTM network with the transpose convolution neural network to forecast the development of tunnel fires. A temperature field prediction of 60 s in advance was achieved with high accuracy of 97%. Therefore, the strong non-linear fitting capability of the LSTM network is promising in conducting structural parameter identification in order to use the temperature data to obtain the hard-to-measure KMPPs.

This study proposes a method for real-time prediction of hard-to-measure KMPPs for early warning of fire-induced collapse using ML. The rest of this paper is organized as follows: Section 2 introduces the ML framework using the LSTM network, including the inputs, outputs, network architecture, and the learning method. Section 3 provides a numerical example to illustrate the application process of the scheme, and two agents are trained to investigate the importance of uncertain parameter identification. Section 4 evaluates the performances of two ML models and discusses the further application of the proposed method in collapse state monitoring and collapse time prediction.

## 2 ML framework

### 2.1 Problem background

Early warning of the fire-induced collapse at fire rescue scenes includes the real-time acquisition of the current state and prediction of the remaining time of the burning frame before the collapse. Through theoretical, experimental, and numerical analysis of the collapse behavior of steel portal frames under fire, the displacement and displacement velocity of key joints were found to have a specific and *quantitative* relationship with the collapse state, thus selected as KMPPs for early warning. Specifically, for single-span steel portal frames, the displacements at the apex and eaves and corresponding displacement velocities were selected as KMPPs, as shown in Fig. 2.

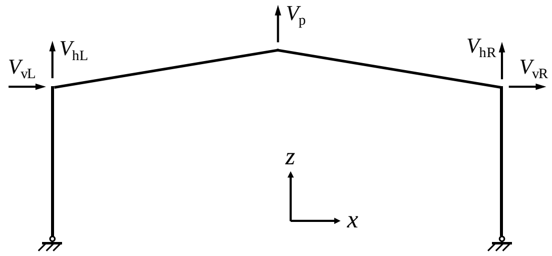


Fig. 2 KMPPs of single-span steel portal frames [13].

The fire-induced collapse process of steel portal frames can be divided into 4 states according to the variation laws of real-time KMPPs-time curves: safety state, 1st warning state, 2nd warning state, and 3rd warning state. The 4 collapse states are distinguished by 3 warning levels, as shown in Fig. 3. Taking the overall collapse mode as an example, the KMPPs-time curves are shown in Fig. 4, where the characteristic points in KMPPs-time curves were defined as early-warning points. The occurrence of each warning level can be determined according to the occurrence of early-warning points, as tabulated in Table 1.

Table 1 Determination of collapse state based on KMPPs [13].

| Collapse state | Occurrence criteria | Definition of points |
|---|---|---|
| Safe stage | No early-warning points occur | *A*: $V_{\mathrm{p}}$ reaches its peak value |
| 1st warning state | Occurrence of point *A* | *B*: $V_{\mathrm{p}}$ decreases to 0 |
| 2nd warning state | Occurrence of one point *C*, *D* or *E* | *C*: $\dot{V}_{\mathrm{p}}$ reaches 10 times of $\dot{V}_{\mathrm{p}}^{A,B}$ |
| 3rd warning state | Occurrence of two points *C*, *D*, *E* | *D*: $V_{\mathrm{hL}}$ reaches its peak value or $\dot{V}_{\mathrm{hL}}$ reaches 10 times of $\dot{V}_{\mathrm{hL}}^{A,B}$ |

Definitions:

$\dot{V}_{\mathrm{p}}^{A,B}$ : average value of $\dot{V}_{\mathrm{p}}$ from point *A* to point *B*

$\dot{V}_{\mathrm{hL}}^{A,B}$ : average value of $\dot{V}_{\mathrm{hL}}$ from point *A* to point *B*

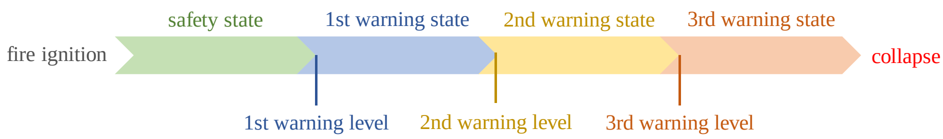


Fig. 3 Collapse process of single-span steel portal frames under fire.

At the *i*th warning level ($i$ = 1, 2, 3), the remaining collapse time $T_i^{\mathrm{R}}$ can be predicted as

$$T_i^{\mathrm{R}} = t_i^{\mathrm{M}} \cdot T_i^{\mathrm{M}} \tag{1}$$

where $t_i^{\mathrm{M}}$ is the ratio of remaining collapse time to fire exposed time at the *i*th warning level, and $T_i^{\mathrm{M}}$ is the fire exposed time at the *i*th warning level. $T_i^{\mathrm{R}}$ and $T_i^{\mathrm{M}}$ are determined based on measurements while $t_i^{\mathrm{M}}$ is a predetermined probability-based value. Parameter analysis on fire and structural uncertainties such as heating conditions, fire protection levels, load ratios and geometry dimensions of frames indicate that $t_i^{\mathrm{M}}$ vary in a certain range with these uncertainties. Therefore, reliability theory coupled with Monte Carlo Sampling were adopted to quantitatively consider the influence of this uncertainties on $t_i^{\mathrm{M}}$. Detailed discussion about the early-warning theory of fire-induced of steel portal frames can be referred to in [13, 14]. Since the early-warning theory is quantitative and is of reliability significance, we can conclude that the decisions facilitated by the early-warning theory are more accurate and reliable than existing experience-based decisions.

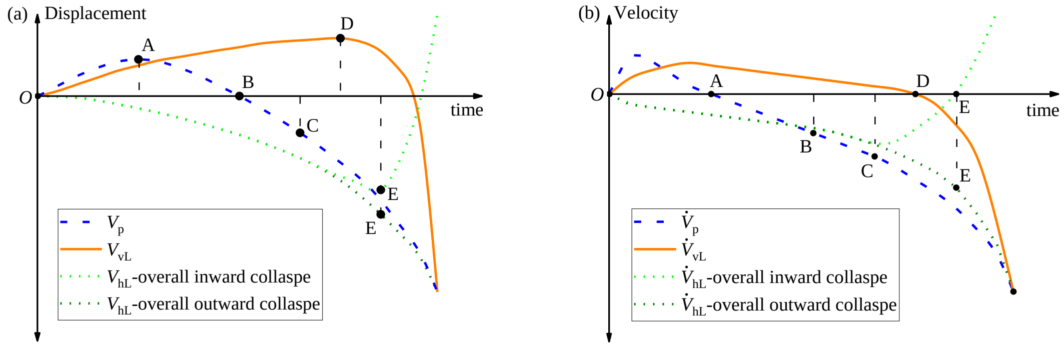


Fig. 4 KMPP-time curves of single-span steel portal frames under fire [13]. (a) Displacement-time curves. (b) Displacement velocity-time curves.

To sum up, the essential of the early warning theory of fire-induced collapse is using the variation law of real-time KMPPs, i.e., displacements at key joints, to reflect the collapse state of the burning structure. Nonetheless, some of the joints are located at the top of the structure. Although it is possible to accurately measure their displacement directly using the microwave radar in a scaled specimen, the measurement scheme will be challenging for real structures since the radar must be placed on the ground. Hence, the problem that this paper aims to resolve is making the hard-to-measure KMPPs easy to obtain, i.e., making the KMPPs fully satisfy requirement R3.

## 2.2 Inputs and outputs

Parameter identification is a hot topic in structural health monitoring [37–39], where the damage to the structure can be identified by the structural responses, which implicitly contain the variation in effective material properties and conditions. This concept can be applied to resolve the problem that the temperature itself cannot reflect the uncertain structural parameters at fire scenes, as some of the KMPPs are easy to measure, e.g., the displacements of the joints located on the wall of the structure. In specific, the easy-to-measure displacements can be used for structural parameter identification, while the easy-to-measure temperature can be used to represent the fire scenario. As the structural parameters and the fire scenario of a specific structure are determined, its structural response can be uniquely determined, as stated in Section 1.

Fig. 5 exhibits the flowchart of the concept mentioned above, where the easy-to-measure temperatures and displacements are used as the inputs, and the outputs are the hard-to-measure displacements. The ultimate goal is to evaluate the collapse state of the burning structure according to the early warning theory [13, 14], using the KMPPs, i.e., both the easy-to-measure and hard-to-measure displacements. Note that the ML model can be trained offline using numerical simulation results, and the computational cost of the trained ML model is significantly smaller than traditional FE analysis; hence, all the KMPPs can be easy to obtain with the trained ML model.

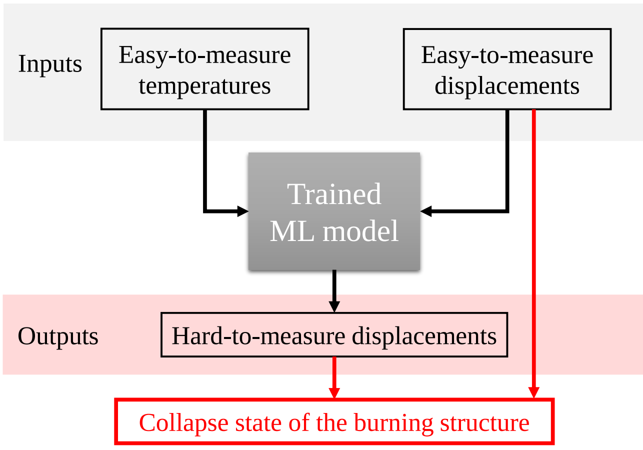


Fig. 5 Flowchart of the concept of the ML problem.

## 2.3 LSTM cell

The LSTM layer consists of a series of LSTM cells to map the non-linear relationship of time series data. Fig. 6 shows the detailed structure of a typical LSTM cell, which contains the cell state, hidden state, and three gates (i.e., forget gate, input gate, and output gate, denoted by subscripts 'F,' 'I,' and 'O,' respectively) for information filtering. In Fig. 6, $\mathbf{x}^{(t)}$ and $\mathbf{y}^{(t)}$ are the input and output at the $t$th time step, respectively; **w** and **b** with various subscripts indicate the weights and biases of the corresponding gates, respectively; '$\sigma$ (the sigmoid function)' or 'tanh' is the activation function of the gate.

It is notable that the cell state is the essential difference between LSTM and traditional RNN, as it runs straight down the LSTM chain to avoid the leak of long-term historical information. At the $t$th time step, the cell state $\mathbf{c}_t$ is updated as

$$\mathbf{c}_t = \left(\mathbf{F}_t \odot \mathbf{c}_{t-1}\right) + \left(\mathbf{I}_t \odot \tilde{\mathbf{C}}_t\right) \tag{2}$$

where $\odot$ denotes the Hadamard product; $\tilde{\mathbf{C}}_t$ is an intermediate state containing the new memory:

$$\tilde{\mathbf{C}}_t = \tanh\left(\mathbf{w}_{\mathrm{C}}\left[\mathbf{h}_{t-1}, \mathbf{x}^{(t)}\right] + \mathbf{b}_{\mathrm{C}}\right) \tag{3}$$

where $\mathbf{h}_{t-1}$ is the hidden state at the $(t-1)$th time step; $\mathbf{w}_{\mathrm{C}}$ and $\mathbf{b}_{\mathrm{C}}$ are the weights and biases of the neuron for calculating $\tilde{\mathbf{C}}_t$. $\mathbf{F}_t$ and $\mathbf{I}_t$ are the outputs of the forget gate and input gate, respectively:

$$\mathbf{F}_t = \sigma\left(\mathbf{w}_{\mathrm{F}}\left[\mathbf{h}_{t-1}, \mathbf{x}^{(t)}\right] + \mathbf{b}_{\mathrm{F}}\right) \tag{4}$$

$$\mathbf{I}_t = \sigma\left(\mathbf{w}_{\mathrm{I}}\left[\mathbf{h}_{t-1}, \mathbf{x}^{(t)}\right] + \mathbf{b}_{\mathrm{I}}\right) \tag{5}$$

The hidden state $\mathbf{h}_t$ of the LSTM cell serves as the output at the current time step and input at the next time step:

$$\mathbf{h}_t = \mathbf{O}_t \odot \tanh\left(\mathbf{c}_t\right) \tag{6}$$

where $\mathbf{O}_t$ is the output of the output gate:

$$\mathbf{O}_{\mathrm{t}} = \sigma\left(\mathbf{w}_{\mathrm{O}}\left[\mathbf{h}_{\mathrm{t-1}}, \mathbf{x}^{(\mathrm{t})}\right] + \mathbf{b}_{\mathrm{O}}\right) \tag{7}$$

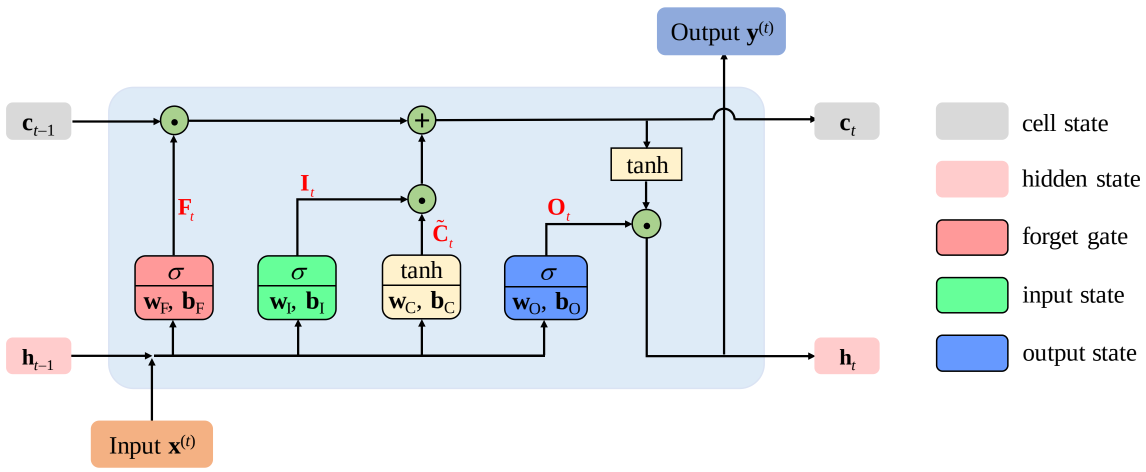


Fig. 6 Detailed structure of an LSTM cell at the $t$th time step.

By introducing the three gates mentioned before, the LSTM network can successfully extract the key features of long-term time series data and can avoid the gradient vanishing existing in traditional RNNs.

## 2.4 Network architecture

With the strong capability of non-linear fitting of time series data, the LSTM layers, containing a number of LSTM cells, are incorporated with fully-connected (FC) layers to form the network in this study, as shown in Fig. 7. In Fig. 7, $t_{\max}$ is the length of the time series data used for the training, $n_{\mathrm{th}}$ is the number of easy-to-measure temperatures, $n_{\mathrm{md}}$ is the number of easy-to-measure displacements, $n_{\mathrm{pd}}$ is the number of hard-to-measure displacements, and these parameters are predetermined for the training of a specific structure; $n_b$ is the batch size used for training, $n_f$ is the size of the hidden state, and these parameters are hyperparameters which need to be tuned according to the performance of the trained agent; 'ReLU' is the Rectified Linear Unit activation function for strengthening the nonlinear fitting ability; 'Dropout' indicates that a certain percent of neurons within the network will be omitted during the current training step in order to avoid overfitting [40, 41]. To summarize, the network shown in Fig. 7 realizes the mapping from a sample of inputs $\mathbf{X}=\left\{\mathbf{x}^{(1)},\mathbf{x}^{(2)},\ldots,\mathbf{x}^{(t_{\max})}\right\}^{\mathrm{T}}\in\mathbb{R}^{t_{\max}\times(n_{\mathrm{th}}+n_{\mathrm{md}})}$ into the corresponding sample of outputs $\mathbf{Y}=\left\{\mathbf{y}^{(1)},\mathbf{y}^{(2)},\ldots,\mathbf{y}^{(t_{\max})}\right\}^{\mathrm{T}}\in\mathbb{R}^{t_{\max}\times n_{\mathrm{pd}}}$, where $\mathbf{x}_i$ and $\mathbf{y}_i$ are the $i$th element within the time series data ($i$ = 1, 2, …, $t_{\max}$).

Notably, the size of the LSTM layer is independent of $t_{\max}$, indicating that the length of the time series in practical use can be different from that used in training.

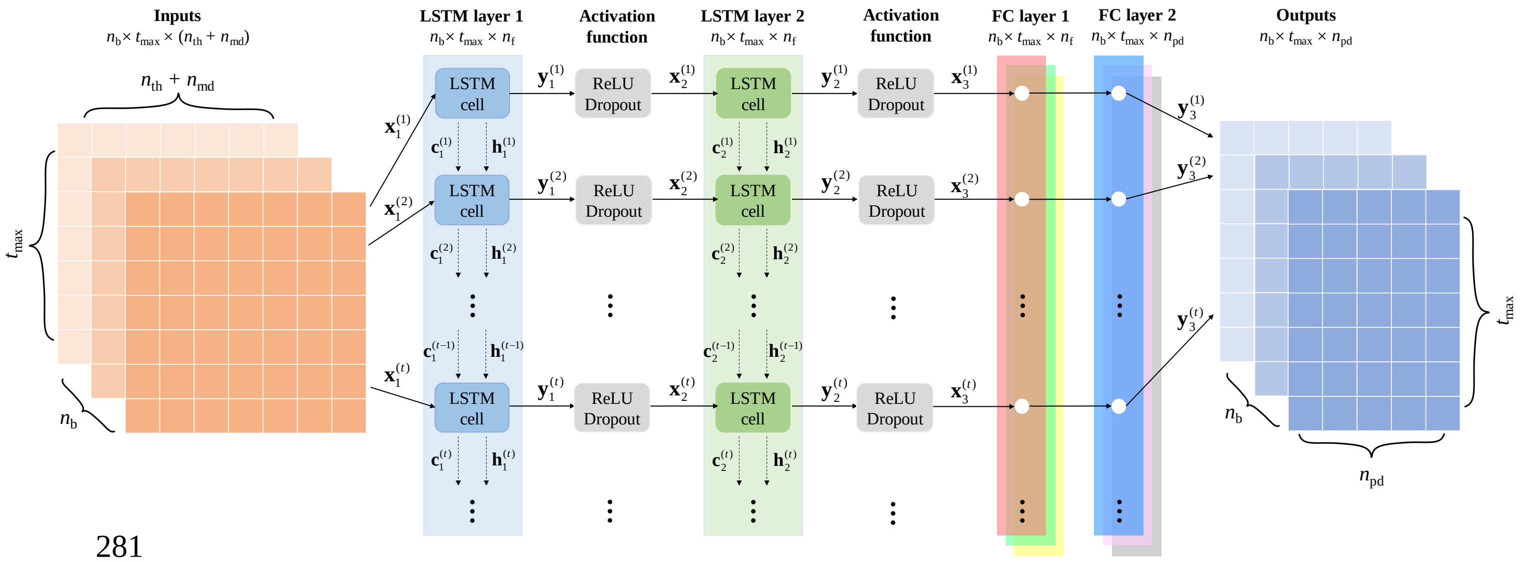


Fig. 7 Network architecture.

## 2.5 Learning method

The learning method adopted herein is to update the network parameters during the training phase, i.e., the weights and biases, in order to improve the non-linear fitting ability of the network.

Traditional Stochastic Gradient Decent (SGD) [42] method updates network parameters $\boldsymbol{\theta}$ by

$$\boldsymbol{\theta}^{(i)}=\boldsymbol{\theta}^{(i-1)}-\eta\mathbf{g}^{(i)} \tag{8}$$

where $\boldsymbol{\theta}^{(i)}$ is the network parameters at the $i$th iteration step; $\eta$ is the learning rate; $\mathbf{g}^{(i)}$ is the gradient of the loss function $J$ with respect to the network parameters at the $i$th iteration step, which can be calculated by the backpropagation algorithm. The loss function is denoted by the error between the predicted and target output of the network.

Typical loss functions include the L1 loss, mean squared error (MSE) loss, mean squared logarithmic error loss. The learning rate of the SGD method remains constant throughout the training phase, which brings about severe problems. In specific, a small learning rate results in slow convergence, while a large learning rate leads to violent oscillation near the optimum (either global or local) parameter set $\boldsymbol{\theta}^*$.

Improved learning methods like AdaGrad [43] can adjust learning rate automatically according to historical gradients:

$$\boldsymbol{\theta}^{(i)} = \boldsymbol{\theta}^{(i-1)} - \frac{\eta}{\sqrt{\sum_{j=1}^{i}\left[\mathbf{g}^{(j)} \odot \mathbf{g}^{(j)}\right] + \varepsilon}} \odot \mathbf{g}^{(i)} \tag{9}$$

where $\varepsilon$ is a sufficiently small positive number to prevent parameter explosion. Compared with the SGD method, the actual learning rate of AdaGrad decreases with the accumulation of gradients in training. Nonetheless, further analysis indicates that the actual learning rate will approach zero if the training phase is too long, as the denominator in Eq. (9) can be very large.

In order to resolve this problem, the Root Mean Square Propagation (RMSProp) [44] is proposed to conditionally throw out historical gradients in the parameter updating process:

$$\boldsymbol{\theta}^{(i)} = \boldsymbol{\theta}^{(i-1)} - \frac{\eta}{\sqrt{\mathbf{v}^{(i)} + \varepsilon}} \odot \mathbf{g}^{(i)} \tag{10}$$

where $\mathbf{v}^{(i)}$ is the second raw moment estimate of gradients:

$$\mathbf{v}^{(i)} = \beta \mathbf{v}^{(i-1)} + (1-\beta)\left[\mathbf{g}^{(i)} \odot \mathbf{g}^{(i)}\right] \tag{11}$$

in which $\beta$ is a hyperparameter for weighted average.

Besides, Adam is a new stochastic optimization algorithm proposed by Kingma and Ba [45] for updating $\boldsymbol{\theta}$. It combines the ability of AdaGrad to deal with sparse gradients and the ability of RMSProp to deal with non-stationary objectives. At $i$th training iteration, $\boldsymbol{\theta}$ is updated as

$$\boldsymbol{\theta}^{(i)} = \boldsymbol{\theta}^{(i-1)} - \frac{\eta}{\sqrt{\frac{\mathbf{v}^{(i)}}{1-\beta^k} + \varepsilon}} \frac{\mathbf{m}^{(i)}}{1-\beta_1^k} \tag{12}$$

where $\beta_1^k$ and $\beta^k$ are the $k$th power of the hyperparameters $\beta_1$ and $\beta$, respectively; $\mathbf{m}^{(i)}$ is the biased first-moment estimate of gradients:

$$\mathbf{m}^{(i)} = \beta_1 \mathbf{m}^{(i-1)} + (1-\beta_1)\mathbf{g}^{(i)} \tag{13}$$

Adam is recommended as the learning method of the proposed ML framework due to its robustness on complex optimization problems, fewer requirements of memory, and ease of implementation [46].

## 3 Numerical example

### 3.1 Geometric information and FE model

As a representative example, a single-span steel portal frame is designed to illustrate the application and accuracy of the proposed ML framework. The frame was designed according to the Chinese code [47], with pinned column bases and without fire protection. The frame has 12 bays with an interval of 6 m and 1 span of 24 m, as shown in Fig. 8. The detailed geometric information of steel components is shown in Table 2.

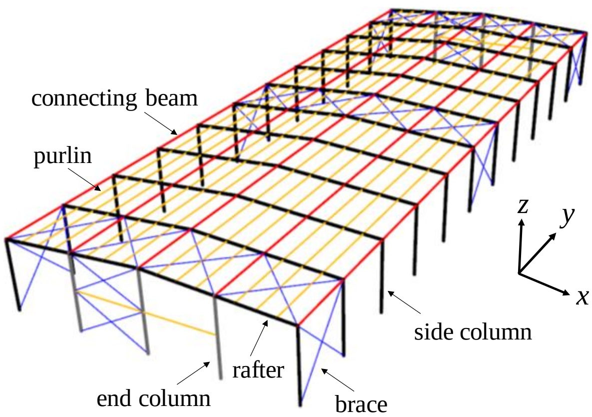


Fig. 8 Layout of the portal frame.

Table 2 Section information of steel members.

| Member type | Cross-section (unit: mm) |
|---|---|
| side column | H500×250×6×10 |
| end column | H250×175×4.5×6 |
| rafter | H600×180×6×8 |
| purlin | H200×100×3.2×4.5 |
| connect beam | Ø180×5 |
| brace | Ø22 |

The dataset for training the ML agent will be generated using thermal-structural coupling analysis in the general FE software ABAQUS [48]. The two-node Timoshenko beam element B31 is used to model the steel members. An element mesh size of 0.15 m is used for rafters and columns, while an element mesh size of 0.3 m is used for other secondary members. Two load steps are set in the FE analysis:

S1 Apply dead loads to the frame at ambient temperature;

S2 Heat the frame according to a preset scheme with the applied load until it collapses.

The detailed validation of the FE model is referred to in literature [22].

### 3.2 Uncertain parameters

Here we note again that the uncertain parameters under fire conditions include the load intensity and distribution, material properties, and the fire scenario. These parameters will be taken as random variables in the preparation of the training dataset according to the following principles:

(1) Load intensity and distribution

The horizontal wind load is ignored for single-span steel portal frames due to its little effect on the structural fire response [49]. The vertical load, which can greatly influence the fire resistance, is assumed to be uniformly distributed on each rafter, as shown in Fig. 9. However, the line load intensity on the rafters at the $i$th bay, i.e., $q_{\mathrm{L}}^{i}$ and $q_{\mathrm{R}}^{i}$, are assumed to obey the uniform distribution of $U(0.3q_{\mathrm{u}}, 0.5q_{\mathrm{u}})$, where $q_{\mathrm{u}}$ refers to the ultimate load capacity of the frame under uniformly distributed load at ambient temperature.

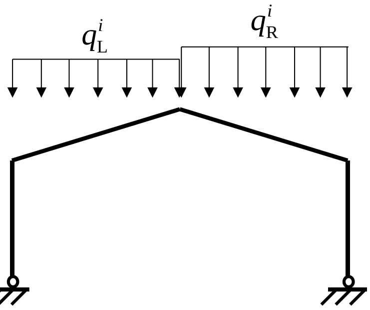


Fig. 9 Load distribution on rafters at the $i$th bay.

(2) Material properties

The Q235 steel is adopted as the material of all the components. The yield strength $f_{\mathrm{y}}$, and ultimate strength $f_{\mathrm{u}}$ of steel at ambient temperature are assumed to obey uniform distribution regarding their design values (with the subscript 'd'), as tabulated in Table 3. Note that the elastic modulus $E$ and elevated-temperature reduction coefficient of the material properties of steel are taken as determinate values according to Eurocode 3 [50], since the reduction in material properties obeys an objective law.

Table 3 Steel properties at ambient temperature.

| Material property | Probability distribution | Designed value |
|---|---|---|
| $f_{\mathrm{y}}$ | $U(0.9f_{\mathrm{y,d}}, 1.1f_{\mathrm{y,d}})$ | $f_{\mathrm{y,d}}$ = 235 MPa |
| $f_{\mathrm{u}}$ | $U(0.9f_{\mathrm{u,d}}, 1.1f_{\mathrm{u,d}})$ | $f_{\mathrm{u,d}}$ = 294 MPa |

(3) Fire scenarios

Without loss of generality, the fire is assumed to be ignited at the fourth bay for simplification. The randomness of the fire scenarios will be considered by different cases of fire spread along the span and bay. A total of 39 fire scenarios (denoted as FS1–FS39), which are the combinations of 12 heating conditions along the span and 4 heating conditions along the bay, are considered. Since the temperature of steel members along the length is uneven in real fires, temperature partitions are adopted herein for each member. Here we note that as the goal of the ML framework is learning the parameter identification and the mapping relationship from the temperature to the structural response, even though the actual temperature distribution does not correspond to the specified one, the trained agent is still expected to produce a satisfactory prediction, which will be validated in Section 4. Thus, regarding the current numerical example, the heating conditions along the span and the bay are tabulated in Tables 4 and 5, respectively, where T1 and T2 are uniform temperature partitions. Steel members in T2 will retain the ambient temperature, while members in T1 will be uniformly heated. The corresponding partition numbers are defined in Figs. 10 and 11.

Table 4 Heated partitions of different heating conditions along the span.

| Heating condition | T1 | T2 |
|---|---|---|
| S1 | H1, H2 | H3–H8 |
| S2 | H1–H3 | H4–H8 |
| S3 | H1–H4 | H5–H8 |
| S4 | H3, H4 | H1–H4, H5–H8 |
| S5 | H3–H5 | H1, H2, H6–H8 |
| S6 | H2–H5 | H1, H6–H8 |
| S7 | H2–H6 | H1,H7, H8 |
| S8 | H1–H6 | H7, H8 |
| S9 | H4, H5 | H1–H3, H6–H8 |
| S10 | H3–H6 | H1, H2, H7–H8 |
| S11 | H2–H7 | H1, H8 |
| S12 | H1–H8 | / |

Table 5 Heated partitions of different heating conditions along the bay.

| Heating conditions along the bay | T1 | T2 |
|---|---|---|
| B1 | F3–F5 | F1, F2, F6–F12 |
| B2 | F2–F6 | F1, F7–F12 |
| B3 | F1–F7 | F8–F12 |
| B4 | F1–F12 | / |

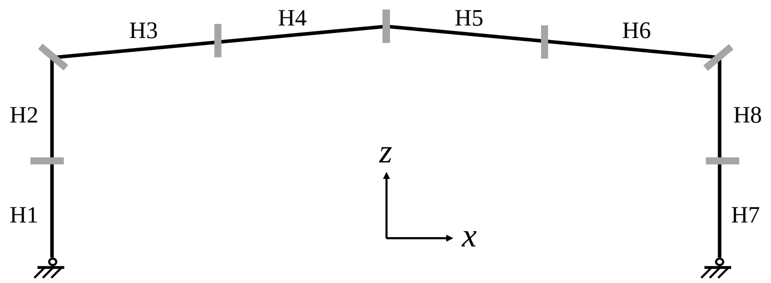


Fig. 10 Partition of steel members along the span.

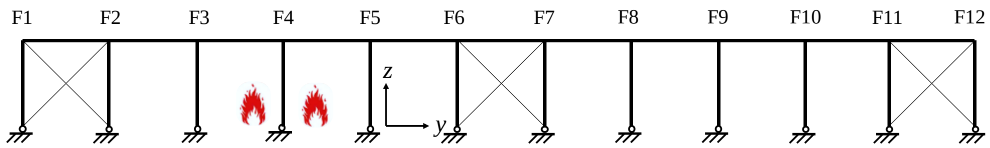


Fig. 11 Partition of steel members along the bay.

Single-layer steel portal frames are one of the large-space structures, and the fire scenario is localized. For simplification in this example, the localized fire is assumed to be the Eurocode parametric fire [51] with a duration of 60 min, and the air temperature can be calculated as

$$T_{\mathrm{g}}(t)=20+1325\left[1-0.324\mathrm{e}^{-0.2\left(\frac{t}{60}\cdot\Gamma\right)}-0.204\mathrm{e}^{-1.7\left(\frac{t}{60}\cdot\Gamma\right)}-0.472\mathrm{e}^{-19\left(\frac{t}{60}\cdot\Gamma\right)}\right] \tag{14}$$

where $T_{\mathrm{g}}$ is the air temperature (°C), and $t$ is the fire duration (min). Γ is a dimensionless parameter related to the opening factor $O$ ($\mathrm{m}^{1/2}$) and the thermal absorptivity $b$ ($\mathrm{J\cdot m^{-2}\cdot s^{-1/2}\cdot °C^{-1}}$) of the burning space:

$$\Gamma=\frac{(O/b)^2}{(0.04/1160)^2} \tag{15}$$

Note that other reliable fire models can also be used for different kinds of fire sources.

For unprotected steel members, the steel temperature can be calculated based on an iterative process [52]:

$$T_{\mathrm{s}}(t+\Delta t)=\alpha\cdot\frac{1}{c_{\mathrm{s}}\rho_{\mathrm{s}}}\cdot\frac{F}{V}\cdot\left[T_{\mathrm{g}}(t)-T_{\mathrm{s}}(t)\right]\Delta t+T_{\mathrm{s}}(t) \tag{16}$$

where $T_{\mathrm{s}}$ is the steel temperature (°C), $c_{\mathrm{s}}$ is the specific heat of steel ($\mathrm{J\cdot kg^{-1}\cdot °C^{-1}}$), $\rho_{\mathrm{s}}$ is the unit mass of steel ($\mathrm{kg\cdot m^{-3}}$), $F$ is the surface area of the steel member per unit length ($\mathrm{m^2/m}$), $V$ is the volume of the steel member per unit length ($\mathrm{m^3/m}$), and $\Delta t$ is the time interval. $\alpha$ is the combined heat transfer coefficient ($\mathrm{W\cdot m^{-1}\cdot °C^{-1}}$) related to the convective and radiative heat transfer coefficients $\alpha_{\mathrm{c}}$ and $\alpha_{\mathrm{r}}$:

$$\alpha=\alpha_{\mathrm{c}}+\alpha_{\mathrm{r}} \tag{17}$$

$$\alpha_r = \varepsilon_r \cdot \sigma \cdot \frac{\left(T_g + 273\right)^4 - \left(T_s + 273\right)^4}{T_g - T_s} \tag{18}$$

in which $\varepsilon_r$ is a dimensionless parameter related to the combined emissivity, and $\sigma$ is the Stephan-Boltzman constant which should be taken as $5.67\times10^{-8}$ W/(m$^2$·°C$^4$).

The parameter Γ controls the shape of the air temperature-time curve, and a large Γ indicates a high heating rate. To further consider the randomness of the fire scenario, Γ is assumed to obey $U(0.5, 5)$. In this case, the heated rafters will reach a temperature between 800°C to 1200°C, as shown in Fig. 12.

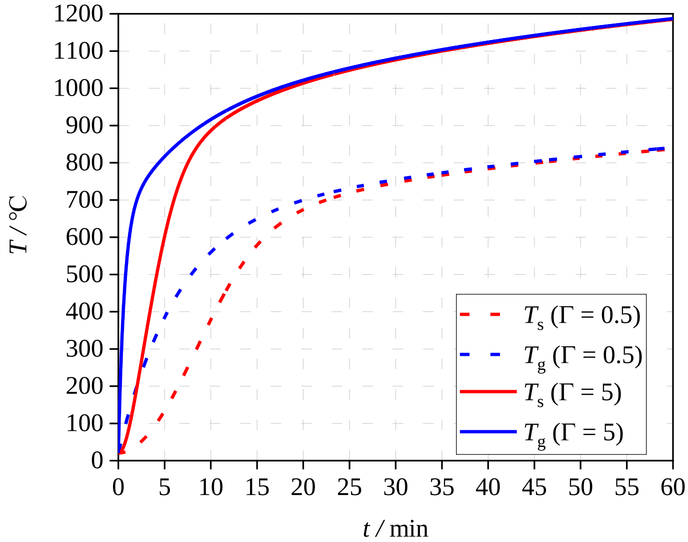


Fig. 12 Air and steel temperature-time curves based on Eurocode parametric fire.

## 3.3 Key data involved in the ML model

Preparation of the dataset is a crucial step in ML. As described in Section 2.2, the KMPPs, i.e., displacement of key joints and the temperature of key members, will be extracted from FE analysis as key data involved in training.

(1) Selection of KMPPs

For single-span steel portal frames, the lateral constraints provided by the purlins can be ignored when calculating the vertical displacement of the rafter, as there is a significant difference in the stiffness. Ji *et al.* [13] indicated that the KMPPs of single-span steel portal frames are the displacements of apex and eaves in the *x*-*z* plane of the bay, for the evaluation of the collapse state under fire, as shown in Fig. 13. In Fig. 13, $V_{vL}$ and $V_{hL}$ are the vertical and horizontal displacements of the left eave, respectively; $V_{vR}$ and $V_{hR}$ are the vertical and horizontal displacements of the right eave, respectively; $V_p$ is the vertical displacement of the apex.

However, we need to highlight that it is difficult to judge in time which bay is the most seriously affected in real fire conditions. Therefore, it is reasonable to monitor as many potential displacements of the apex and eaves of each bay under fire as possible in order to evaluate the collapse state of the burning frame based on the bay with the largest deformation. In this way, the same ML framework needs to be adopted multiple times at the design phase (offline) in order to ensure the real-time prediction of the ML model at fire scenes. As for the numerical example mentioned herein, the fire is assumed to be ignited and spread from the fourth bay. For the sake of simplification, only the 5 key displacements of the fourth bay are adopted as KMPPs for real-time monitoring of the collapse state. $V_{\mathrm{vL}}$ and $V_{\mathrm{hL}}$ are selected as easy-to-measure KMPPs (supposing the radars are located at the left side of the structure as shown in Fig. 13), i.e., part of the inputs, while the rest of the displacements in Fig. 1 are defined as hard-to-measure KMPPs, i.e., the outputs. In this way, the values of $n_{\mathrm{md}}$ and $n_{\mathrm{pd}}$ are 2 and 3, respectively. The reliability of on-site arranged microwave radars for displacement measurement has been proved in literature [53, 54].

(2) Selection of temperatures

Another part of the inputs is the temperature of key members. As the columns and rafters are equally divided into two parts as temperature partitions shown in Fig. 10, a thermocouple is pre-embedded in the middle of each component at each bay. Since there are only 4 heating conditions along the bay of the example frame herein, as shown in Fig. 11, only the temperature information at the 5th, 6th, 7th, and 8th bay is adopted for network training for simplification. The arrangement of the thermocouples is exhibited in Fig. 13, where the total number of thermocouples $n_{\mathrm{th}}$ is 4×8 = 32.

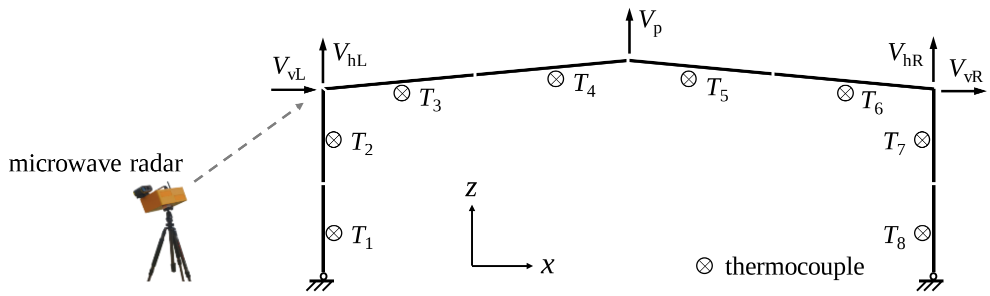


Fig. 13 Arrangement of microwave radars and thermocouples.

### 3.4 ML models and training datasets

In this section, two ML models with different inputs and outputs will be established. By comparing the performance of both models, we would like to illustrate the necessity of conducting parameter identification.

For Model 1, the $t$th element of $\mathbf{X}_j$ and $\mathbf{Y}_j$ are constructed as

$$\mathbf{x}_j^{(t)} = \left\{ V_{\mathrm{hL}}^{(t)}, V_{\mathrm{vL}}^{(t)}, T_1^{(t)}, T_2^{(t)}, \ldots, T_{32}^{(t)} \right\} \tag{19}$$

$$\mathbf{y}_j^{(t)} = \left\{ V_{\mathrm{p}}^{(t)}, V_{\mathrm{hR}}^{(t)}, V_{\mathrm{vR}}^{(t)} \right\} \tag{20}$$

in which $T_i^{(t)}$ represents the $t$th element of the time series data recorded by the $i$th thermocouple ($i$ = 1, 2, …, 32).

500 samples are generated through thermal-structural coupling analysis using the FE model established in Section 3.1. The distributions of uncertain parameters are shown in Fig. 14, where uniform distributions can be assumed. The fire duration is selected as 3600 s with a recording interval $\Delta t$ of 10 s, i.e., $t_{\max}$ = 3600/10 = 360. Here we note again that for Model 1, some of the variables are randomly selected as specified in Section 3.2, and parameter identification is expected to be implicitly conducted by introducing the easy-to-measure KMPPs and temperatures into the inputs.

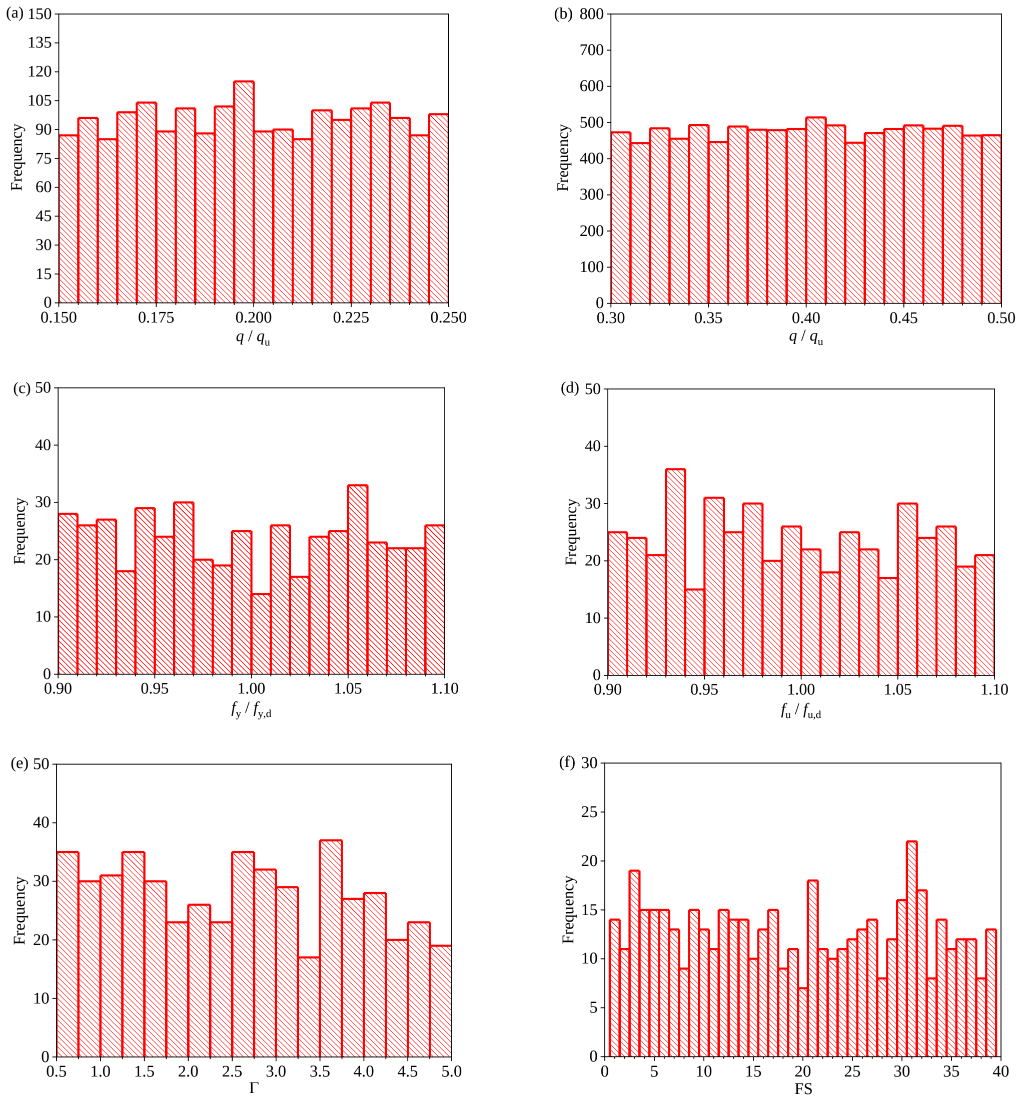


Fig. 14 Distributions of uncertain parameters. (a) Load intensity at 1st and 12th bay. (b) Load intensity at 2nd–11th bay. (c) Yield strength. (d) Ultimate strength. (e) Dimensionless parameter Γ. (f) Fire scenario.

For Model 2, the $t$th element of $\mathbf{X}_{j,\mathrm{c}}$ and $\mathbf{Y}_{j,\mathrm{c}}$ are constructed as

$$\mathbf{x}_{j,\mathrm{c}}^{(t)} = \left\{ T_1^{(t)}, T_2^{(t)}, \ldots, T_{32}^{(t)} \right\} \tag{21}$$

$$\mathbf{y}_{j,\mathrm{c}}^{(t)} = \left\{ V_{\mathrm{hL}}^{(t)}, V_{\mathrm{vL}}^{(t)}, V_{\mathrm{p}}^{(t)}, V_{\mathrm{hR}}^{(t)}, V_{\mathrm{vR}}^{(t)} \right\} \tag{22}$$

500 samples are also generated for the training of Model 2. However, it is obvious that Model 2 cannot deal with uncertain structural parameters. In this case, the intensity of the vertical load is assumed to be a deterministic value of $0.4q_{\mathrm{u}}$. Besides, the elastic modulus, yield strength, and ultimate strength of steel at ambient temperature are also set deterministically as their design values. The fire duration and the recording interval are the same as that of Model 1.

Input for Model 1 | Input for Model 2 | Output for Model 2 | Output for Model 1

| | $t$ / s | $T_1$ / °C | $T_2$ / °C | … | $T_{31}$ / °C | $T_{32}$ / °C | $V_{\mathrm{hL}}$ / mm | $V_{\mathrm{vL}}$ / mm | $V_{\mathrm{p}}$ / mm | $V_{\mathrm{hR}}$ / mm | $V_{\mathrm{vR}}$ / mm |
|---|---|---|---|---|---|---|---|---|---|---|---|
| ambient temperature | 0 | 20 | 20 | … | 20 | 20 | 0 | 0 | 0 | 0 | 0 |
| | 10 | 20 | 20 | … | 20 | 20 | 0 | 0 | 0 | 0 | 0 |
| | 20 | 20 | 20 | … | 20 | 20 | 0 | 0 | 0 | 0 | 0 |
| elevated temperature | 30 | 21.42 | 21.42 | … | 20 | 20 | -0.439 | 0.012 | 0.043 | 0.405 | -0.001 |
| | 40 | 25.53 | 25.53 | … | 20 | 20 | -0.878 | 0.021 | 0.086 | 0.809 | -0.002 |
| | … | … | … | … | … | … | … | … | … | … | … |
| | 3600 | 992.96 | 992.96 | | 20 | 20 | 1281.53 | -815.71 | -4435.17 | -864.53 | -764.53 |

Fig. 15 Illustration of inputs and outputs of Models 1 and 2.

However, the burning frame always collapses before the predefined fire duration of 3600 s, and the collapse time varies with the fire parameters mentioned in Section 3.2. Therefore, the training samples are inconsistent in the time dimension, which brings unnecessary trouble to the integration of training data. In this case, the temperature and displacement data at ambient temperature, i.e., 20°C and 0 mm, are added to the beginning of the time series in order to make the time dimension unified to $t_{\mathrm{max}}$. Fig. 15 gives an illustration of the inputs and outputs of Models 1 and 2 after the data supplement. The samples are then randomly divided into three subsets, including the training dataset with 300 samples, the validation dataset with 100 samples, and the test dataset with 100 samples. Only the training and validation datasets will be involved in updating the learnable parameters based on the learning method described in Section 2.5. Since the uncertain parameters are randomly selected, the test dataset can be regarded as a completely unknown dataset for the evaluation of the trained agent.

## 3.5 Training history

The training of Models 1 and 2 is conducted using TensorFlow in Python. All of the inputs and outputs are scaled within the range of [−1, 1] to improve the performance of the agent. The weights and biases of all LSTM and FC layers are initialized randomly before training. The mean squared error (MSE) is selected as the loss function, and the objective of the training process is to minimize the loss function by adjusting the trainable parameters. The training phase consists of 50000 epochs with a batch size of 128, which means 128 samples in the training dataset are selected randomly in an epoch to update the trainable parameters of the network. As suggested in Section 2.5, Adam is selected as the optimizer. The hyperparameters $\eta$, $\beta_1$, $\beta$, and $\varepsilon$ are set as 0.001, 0.9, 0.999, and $10^{-8}$, respectively.

The history of the losses is shown in Fig. 16 on a logarithmic scale. It can be observed that the loss functions converge at a low value after 10000 epochs. The train loss is larger than the test loss in Fig. 16(b) because the regularization approach 'Dropout' is used in training yet ignored in testing. The training is conducted on a laptop with a CPU of Intel(R) Core(TM) i7-8700k @3.70 GHz and a GPU of NVIDIA GeForce GTX 960. 12 cores with a CPU utilization of 17 % participated in the training. 8.7 G physical memory out of 16 G and 2.8 G GPU memory out of 4 G were included in the training. The computational cost for Models 1 and 2 are 31.4 h and 30.1 h, respectively.

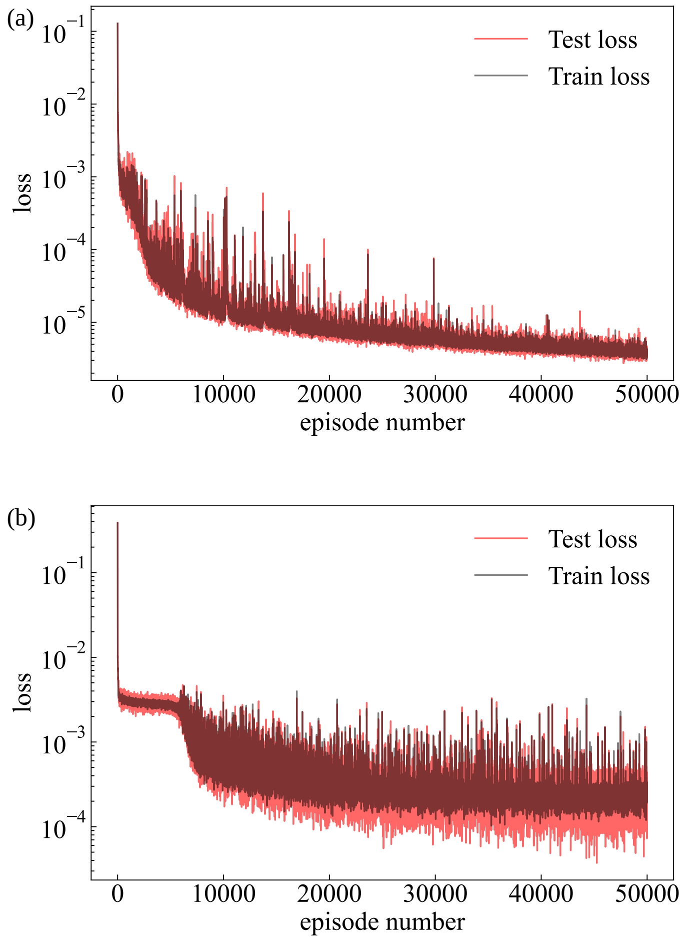


Fig. 16 Training history. (a) Model 1. (b) Model 2.

## 4 Model performance and discussion

In this section, the model performance will be evaluated by comparing the actual and predicted displacement-time curves of the test dataset. Here we note again the test dataset has not participated in the training process and can be regarded as a completely unknown dataset. To quantitatively evaluate the performance of the trained agent, the following indices are introduced:

(1) Correlation coefficient $r$

$$r = \frac{\sum_{t=1}^{t_{\max}} \left[ y_{\text{true}}^{(t)} - \bar{y}_{\text{true}} \right] \left[ y_{\text{pred}}^{(t)} - \bar{y}_{\text{pred}} \right]}{\sqrt{\sum_{t=1}^{t_{\max}} \left[ y_{\text{true}}^{(t)} - \bar{y}_{\text{true}} \right]^2 \sum_{t=1}^{t_{\max}} \left[ y_{\text{pred}}^{(t)} - \bar{y}_{\text{pred}} \right]^2}} \tag{23}$$

(2) Coefficient of determination $R^2$

$$R^2 = 1 - \frac{\sum_{t=1}^{t_{\max}} \left[ y_{\text{pred}}^{(t)} - y_{\text{true}}^{(t)} \right]^2}{\sum_{t=1}^{t_{\max}} \left[ y_{\text{true}}^{(t)} - \bar{y}_{\text{true}} \right]^2} \tag{24}$$

(3) Root mean squared error $RMSE$

$$RMSE = 1 - \sqrt{\frac{\sum_{t=1}^{t_{\max}} \left[ y_{\text{pred}}^{(t)} - y_{\text{true}}^{(t)} \right]^2}{t_{\max}}} \tag{25}$$

where $y^{(t)}$ with various subscripts is the $t$th element of time series data $\mathbf{y}$ and $\bar{y}$ is the average value of $\mathbf{y}$. Subscripts 'true' and 'pred' indicate the actual and predicted time series, respectively. $t_{\max}$ is the length of $\mathbf{y}$. Generally, a satisfactory prediction can be assumed if $r$ is close to 1, $R^2$ is close to 1, or $RMSE$ is close to 0.

### 4.1 Performance of Model 1

For Model 1, the inputs of the test dataset are fed into the trained agent to predict the hard-to-measure KMPPs $V_{\text{p}}$, $V_{\text{hR}}$, and $V_{\text{vR}}$. The distribution histograms of $r$, $R^2$, and $RMSE$ are shown in Fig. 17, where $n$ is the number of samples (with a maximum of 100, which is the same as the number of test samples). It can be observed that the agent can give a precise prediction as the value of $r$ and $R^2$ is greater than 0.8, and the value of $RMSE$ is smaller than 20 mm for most samples, especially for $V_{\text{p}}$ and $V_{\text{hR}}$. Fig. 18 shows a typical comparison case of the actual and predicted displacement-time curves, where satisfactory agreement can be concluded.

However, it is notable that for rare cases, $r$ or $R^2$ is very small for $V_{\text{hR}}$ and $V_{\text{vR}}$.

Further analyses indicate that the frame does not collapse due to low heating rates or load levels. A typical example is shown in Fig. 19, where the frame has small deformation, especially for $V_{vR}$, and a slight data fluctuation will bring significant relative errors according to Eqs. (23) and (24). However, this data fluctuation does not influence the judgment of the collapse state as the trend of the actual and predicted curves are very similar. In this case, *RMSE* is more appropriate than $r$ and $R^2$ for evaluation. On the other hand, *RMSE* is scale-dependent, and an enormous value will be calculated when the ultimate displacement is large, e.g., $V_p$ in Fig. 18. In this case, $r$ and $R^2$ are more appropriate than *RMSE* for evaluation. Based on careful analyses of the results, we recommend that satisfactory performance of the agent can be concluded when the evaluation indices meet the following requirements:

$$(r > \alpha) \cup (R^2 > \beta) \cup (RMSE < \gamma) \tag{25}$$

where $\alpha$, $\beta$, and $\gamma$ are threshold values:

- for high accuracy requirements, $\alpha = 0.9$, $\beta = 0.9$, and $\gamma = 10$ mm;
- for medium accuracy requirements, $\alpha = 0.8$, $\beta = 0.8$, and $\gamma = 20$ mm;
- for low accuracy requirements, $\alpha = 0.7$, $\beta = 0.7$, and $\gamma = 30$ mm.

The percentage of test samples (using Model 1) satisfying the requirements mentioned above is shown in Fig. 20. Since over 90% of the samples meet the high accuracy requirements, it can be concluded that the trained agent has successfully learned the mapping relationship of this specific structure accurately without overfitting, and the orders of magnitude of the prediction results are identical to the true data.

Notably, compared with the fluctuated prediction curves in literature [21], the smoothness of the curves in Fig. 18 indicates the superiority of the application of the LSTM network when dealing with time series data with respect to traditional supervised learning methods.

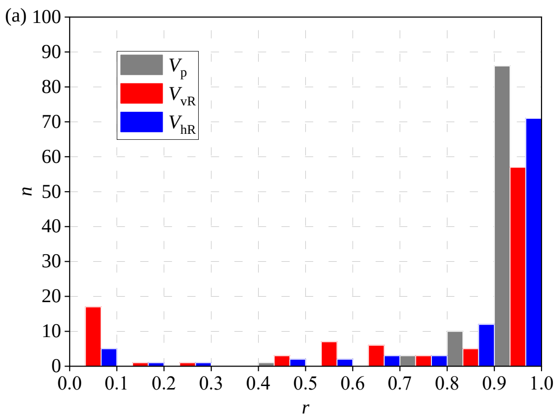

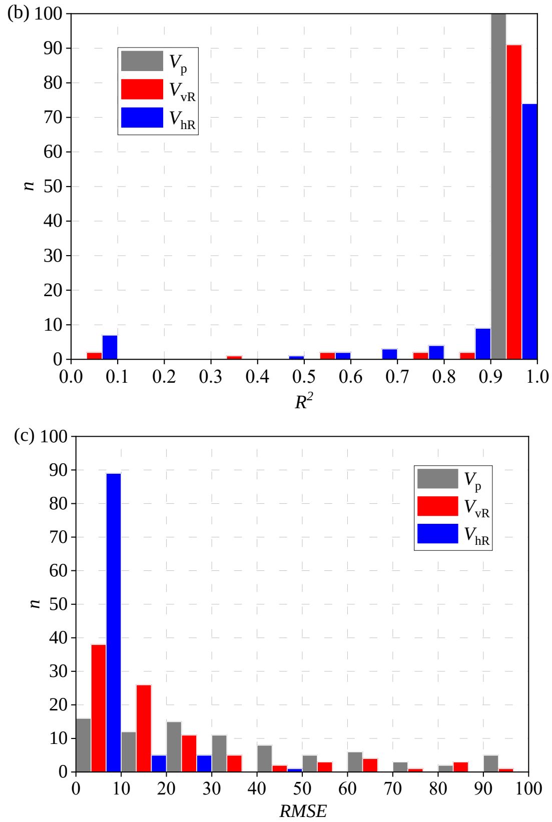


Fig. 17 Evaluation indexes of Model 1 for the hard-to-measure KMPPs.

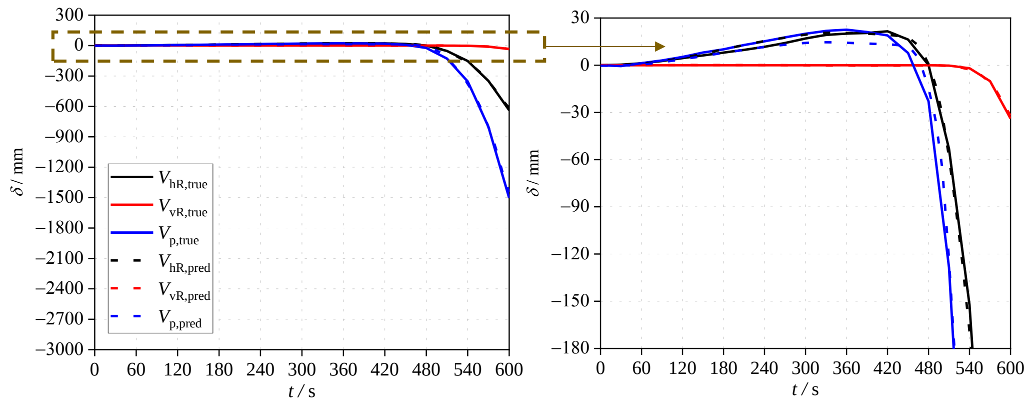


Fig. 18 A typical case of the displacement prediction under large deflections.

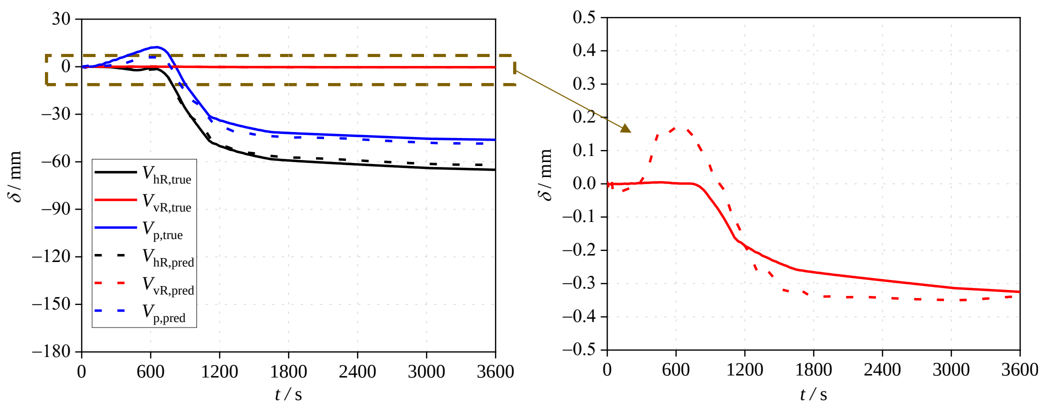


Fig. 19 A typical case of the displacement prediction under small deflections.

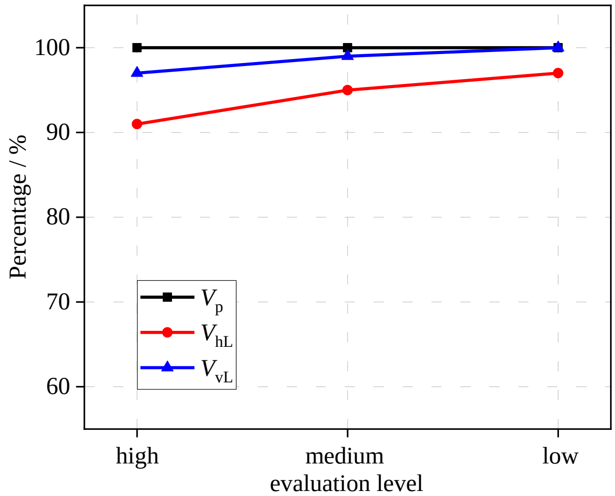


Fig. 20 Performance of Model 1 for the hard-to-measure KMPPs.

We also need to highlight that since the fire scenarios in the test dataset are unknown to the trained agent, i.e., they have not participated in the training process, it can be concluded that the agent has successfully learned the mapping relationship from temperature to structural responses, and can adapt to general building fire scenarios.

Apart from the prediction accuracy, the computational cost is also an important consideration for real-time monitoring in fire rescue. The computational cost for Model 1 to predict a single case of hard-to-measure KMPPs is 0.621 s on the same laptop used for training, which is significantly smaller than the recording interval, i.e., 10 s. Therefore, it is reasonable to use Model 1 at real fire scenes to realize real-time prediction of hard-to-measure KMPPs.

## 4.2 Performance of Model 2

For model 2, the measured temperatures are used as inputs, while all the KMPPs are the outputs as described in Section 3.4. In order to make Models 1 and 2 comparable, the test dataset considering randomness, i.e., the same test dataset used to evaluate Model 1, is used to evaluate the performance of Model 2 in dealing with the uncertain parameters. The performance of the test samples of Model 2 is shown in Fig. 21.

By comparing Figs. 17 and 21, it can be concluded that the regression performance of Model 2 is considerably worse than that of Model 1 when the uncertain parameter identification is ignored, as the percentage in Fig. 21 is smaller than that of Model 1, especially at high accuracy requirements. In other words, the uncertainties in load distribution and material properties will significantly affect the structural response under a specific fire scenario and must not be ignored in early warning of fire-induced building collapse. Specifically, the actual physical model of the burning building cannot be directly determined since the uncertain parameters can differ from their design values. As the easy-to-measure KMPPs implicitly contain the information of the actual values of the uncertain parameters, Model 1 can identify the actual physical model of the burning building through the inputs of easy-to-measure KMPPs, while Model 2 always uses a determined (wrong for most cases) physical model that causes huge errors.

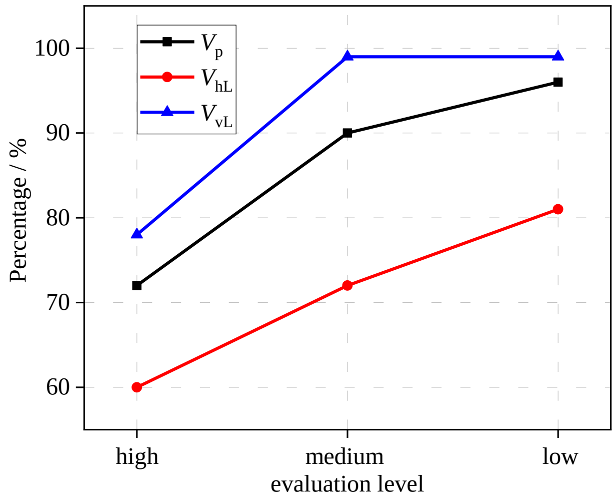


Fig. 21 Performance of Model 2 for different KMPPs.

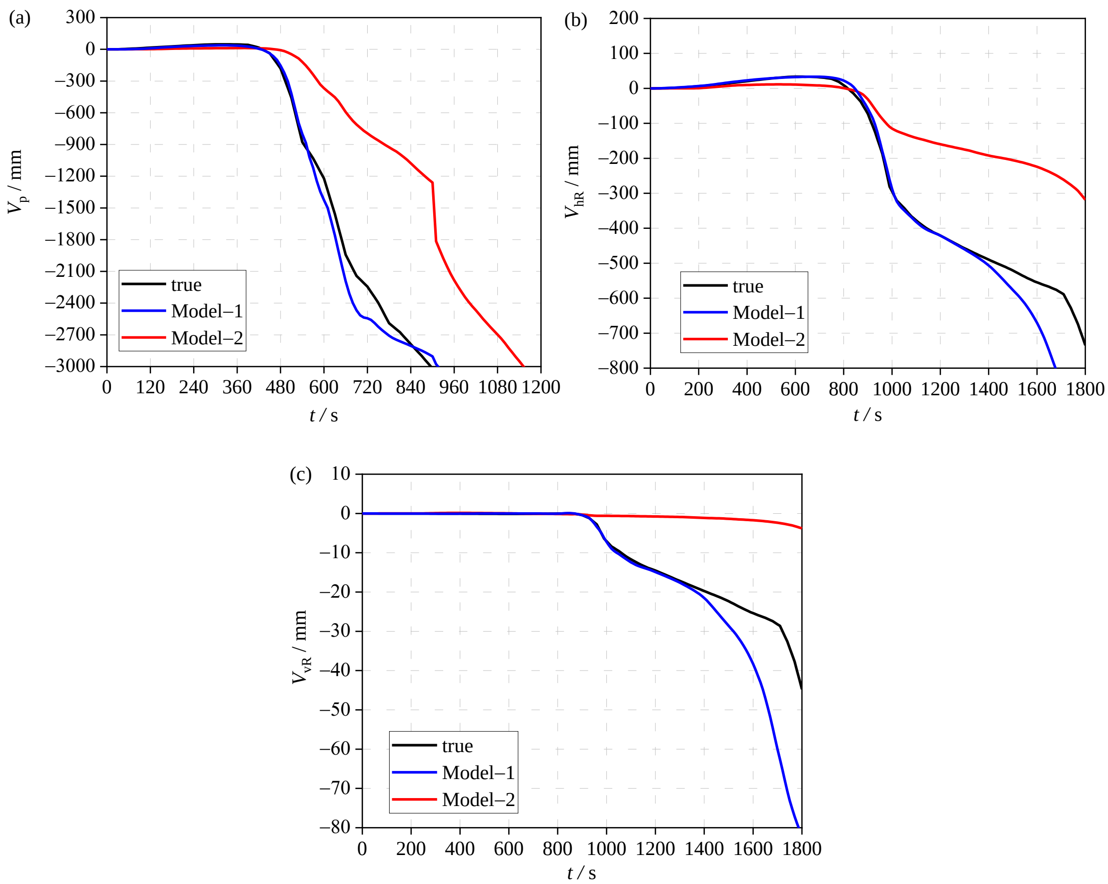


Fig. 22 Typical cases of comparison of actual and predicted displacement-time curves using Model 1 and Model 2. (a) Case 1. (b) Case 2. (c) Case 3.

Fig. 22 shows some typical cases of the comparison of the actual and predicted displacement-time curves using Model 1 and Model 2. It can be observed that Model 2, to a great extent, misjudges the collapse state of the structure, which proves the necessity of considering structural parameter uncertainties in the training of the ML model.

### 4.3 Early warning of fire-induced collapse using the proposed method

Once all the KMPPs are obtained either through field measurement or model prediction, the collapse state of the burning frame can be judged, and the remaining collapse time can also be predicted according to the early warning theory proposed by Li *et al*. [13, 22]. Note that only the KMPP data (measured directly and obtained using the proposed ML approach) are provided to the early-warning algorithm.

To illustrate the application process of the proposed method in real-time early warning of fire-induced collapse, a typical case in the test dataset of Model 1 is adopted herein. At the fire rescue scene, suppose the inputs, i.e., $V_{\mathrm{hL}}$ and $V_{\mathrm{vL}}$, are measured by microwave radars while $V_{\mathrm{p}}$, $V_{\mathrm{hR}}$, and $V_{\mathrm{vR}}$ of the burning frame are predicted by the trained agent (Model 1), as shown in Fig. 23.

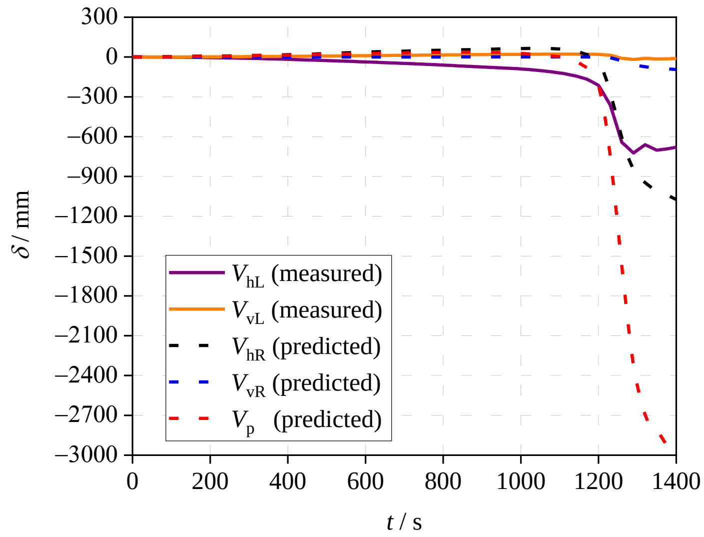


Fig. 23 Measured and predicted KMPPs of a typical frame under fire.

After fire ignition (0 s ~ 600 s), the measured $V_{\mathrm{hR}}$ and predicted $V_{\mathrm{hL}}$ expanded towards opposite directions, as shown in Fig. 24(a). Therefore, an overall collapse mode can be identified for the burning frame according to literature [13]. Since the predicted $V_{\mathrm{p}}$ does not reach its peak value, the collapse state of the frame is safe. At this time, the firefighters can be assured of firefighting and rescue.

When $V_{\mathrm{p}}$ reaches its peak value at about 860 s, as shown in Fig. 24(b), the collapse state changes from the safety state to the 1st warning state, according to Table 1. In this case, the fire has influenced the load-bearing capacity of the heated rafters, and the firefighters should speed up the rescue.

When $V_{vL}$ reaches its peak value at about 1140 s, as shown in Fig. 24(c), the collapse state changes from the 1st warning state to the 2nd warning state, according to Table 1. The fire has affected the load-bearing capacity of the heated columns, and the collapse risk greatly increases. In this case, the firefighters should evacuate from the burning frame to avoid casualties.

When displacement velocity of $V_p$ reaches the critical value at about 1200 s, as shown in Fig. 24(d), the collapse state changes from the 2nd warning state to the 3rd warning state, according to Table 1. In this case, the burning frame is very dangerous, and all the firefighters must evacuate immediately. The prediction results of $V_{vL}$ indicate that the frame will collapse at about 1400 s as the heated rafter has a large deflection of 3 m.

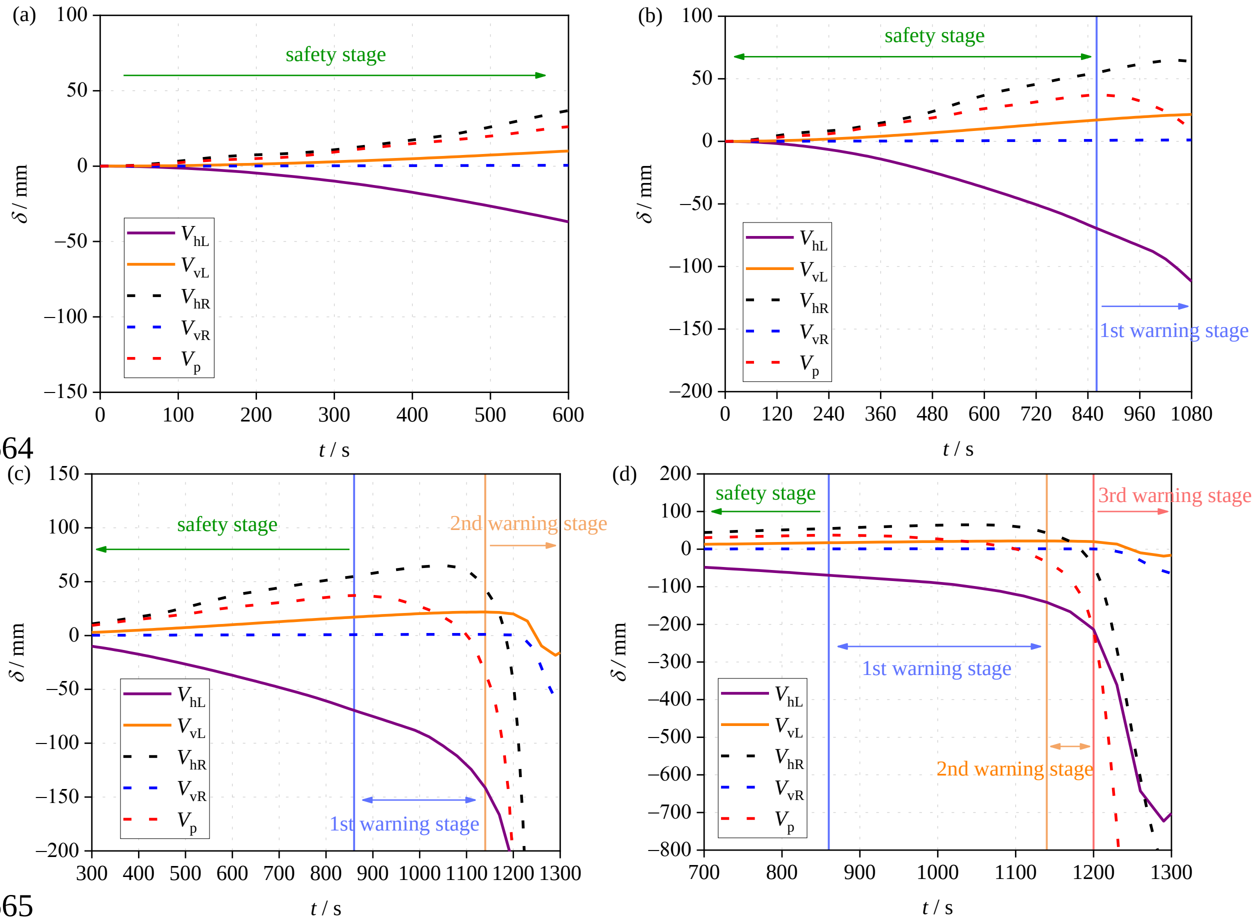


Fig. 24 Collapse state of the burning frame. (a) safety state. (b) 1st warning state. (c) 2nd warning state. (d) 3rd warning state.

Table 6 shows the comparison of the predicted remaining collapse time against the real remaining collapse time of the burning frame at each warning level. The prediction results are satisfactory at high warning levels, while there is a relatively large error at low warning levels, which aligned with previous conclusions [13]. The reason for the prediction error lies in the definition of $t_i^{\mathrm{M}}$. $t_i^{\mathrm{M}}$ has been set as a fixed value based on reliability theory in order to consider the influence of determinate geometric parameters, described in Section 3.1, on the remaining collapse time. The exact ratio of remaining collapse time to fire exposed time can also vary with the determinate geometric parameters and fire parameters. However, we need to highlight that the predicted collapse time will be updated once a higher warning level is raised. In this case, the real-time early warning for fire-induced collapse can still be realized as the predicted remaining time is more accurate for higher early-warning levels. Therefore, it can be concluded that the proposed ML framework (to avoid confusion, for Model 1) is feasible for making the hard-to-measure KMPPs easy to obtain, and the predicted KMPPs can be successfully used for conducting early warning of fire-induced collapse.

Table 6 Prediction of collapse time under each warning level.

| Warning level | $T_i^{\mathrm{M}}$ | $t_i^{\mathrm{M}}$ (reliability level = 80%) | Predicted $T_i^{\mathrm{R}}$ | Real $T_i^{\mathrm{R}}$ |
|---|---|---|---|---|
| 1 | 860 s | 1.703 | 1465 s | 540 s |
| 2 | 1140 s | 0.299 | 341 s | 260 s |
| 3 | 1200 s | 0.176 | 211 s | 200 s |

## 5 Conclusions and future work

This study proposes a real-time prediction method for hard-to-measure KMPPs of fire-induced collapse based on ML. The LSTM network is incorporated with the FC network to predict hard-to-measure KMPPs by inputting easy-to-measure KMPPs and the temperature. A single-span steel portal frame is used as an example to illustrate the training and application process of the proposed method. The findings can be concluded as follows:

(1) Uncertainties, including the load distribution and intensity, structural material properties, and fire scenarios, significantly influence the structural responses at real fire scenes. Therefore, the uncertainties must not be ignored when conducting early warning of fire-induced building collapse;

(2) The uncertainties at real fire scenes can be successfully identified implicitly by selecting the measured temperatures and easy-to-measure KMPPs. In specific, the former and the latter deal with the identification of the actual fire scenario and the structural parameters (i.e., actual load distribution and intensity, material properties), respectively;

(3) For predicting time series data in structural fire engineering, the application of the LSTM network can be superior to other supervised learning methods;

(4) The trained agent considering parameter uncertainties has good robustness in

predicting completely unknown datasets, revealing its prediction capability for real fire scenarios. In this case, the proposed framework can be used as a supplement to traditional displacement measurement means in real fires;

(5) The collapse state of the burning structure can be monitored timely through measured and predicted KMPPs owing to the low computational costs of the trained agent.

As a pioneer study in the real-time prediction of structural responses under fire considering parameter identification, this paper offers an approach to help firefighters judge the collapse risk of burning buildings and make wise decisions.

We need to note that the limitation of this study is that the agent should be individually trained for each building during the design stage. Our future work will increase the applicability of the agent to structures with different sizes and topological relationships by incorporating the graph neural networks.

**Data Availability Statement**

The authors confirm that the data supporting the findings of this study are available within the article and its supplementary materials. Readers can also download the codes and training data via the following link:
https://github.com/percyzhu/LSTM_for_KMPPs.

**References**

[1] Brushlinsky N, Ahrens M, Sokolov S, Wagner P. World Fire Statistics. Center of Fire Statistics, 2021.

[2] Usmani A, Chung Y C, Torero J L. How did the WTC towers collapse: a new theory. Fire Safety Journal, 2003, 38: 501-503.
doi: 10.1016/S0379-7112(03)00069-9

[3] Ali H M, Senseny P E, Alpert R L. Lateral displacement and collapse of single-story steel frames in uncontrolled fire. Engineering Structures, 2004, 26: 593-607.
doi: 10.1016/j.engstruct.2003.12.007

[4] Moss P J, Dhakal R P, Bong M W, Buchanan A H. Design of steel portal frame buildings for fire safety. Journal of Constructional Steel Research, 2009, 65: 1216-1224.
doi: 10.1016/j.jcsr.2008.09.003

[5] Fang C, Izzuddin B A, Nethercot D A. Robustness of steel-composite building structures subject to localized fire. Fire Safety Journal, 2011, 46: 348-363.
doi: 10.1016/j.firesaf.2011.06.001

[6] Egle R, Jamal E. A study on the effect of compartment fire on the behavior of multi-

storey steel framed structures. Fire Technology, 2015, 51: 867-886. doi: 10.1007/s10694-014-0419-0

[7] Kuligowski E D, Zhao X, Lovreglio R, Xu N, Yang K, Westbury A, Nilsson D, Brown N. Modeling evacuation decisions in the 2019 Kincade fire in California. Safety Science, 2022, 146: 105541. doi: 10.1016/j.ssci.2021.105541

[8] Wang D, Yang Y, Zhou T, Yang F. An investigation of fire evacuation performance in irregular underground commercial building affected by multiple parameters. Journal of Building Engineering, 2021, 37: 102146. doi: 10.1016/j.jobe.2021.102146

[9] Kang R, Fu G, Yan J. Analysis of the case of fire fighters casualties in the building collapse. Procedia Engineering, 2016, 135: 343-348. doi: 10.1016/j.proeng.2016.01.140

[10] Jiang L, Zhang Q, Shi J, Li Yang. Statistic study on sacrifices of firefighters in China. Procedia Engineering, 2012, 45: 700-704. doi: 10.1016/j.proeng.2012.08.226

[11] ISO 834-1, Fire-Resistance Tests-Elements of Building Construction Part 1: General Requirements. Geneva, International Organization for Standardization (ISO), 1999.

[12] Jiang J, Wang C, Lou G, Li G Q. Quantitative evaluation of progressive collapse process of steel portal frames in fire. Journal of Constructional Steel Research, 2018, 150: 277-287. doi: 10.1016/j.jcsr.2018.08.020

[13] Ji W, Li G Q, Lou G. Early-warning methods for fire-induced collapse of single-span steel portal frames. Journal of Constructional Steel Research, 2022, 190(2): 107154. doi: 10.1016/j.jcsr.2022.107154

[14] Ji W, Zhu S, Li G Q, Lou G, Jiang S. Approach for early-warning collapse of double-span steel portal frames induced by fire. Fire Safety Journal, 2022, 131: 103628. doi: 10.1016/j.firesaf.2022.103628

[15] Roy K, Lim J B P, Lau H H, Yong P M, Clifton G C, Johnston R P D, Wrzesien A, Mei C C. Collapse behavior of a fire engineering designed single-storey cold-formed steel building in severe fire. Thin-Walled Structures, 2019, 142: 340-357. doi: 10.1016/j.tws.2019.04.046

[16] Lausova L, Kolos I, Michalcova V, Skotnicova I. Numerical analysis of steel portal frame exposed to fire. Procedia Engineering. 2017, 190: 237-242.

doi: 10.1016/j.proeng.2017.05.332

[17] Foster S, Chladna´ M, Hsieh C, Burgess I, Plank R. Thermal and structural behavior of a full-scale composite building subject to a severe compartment fire. Fire Safety Journal, 2007, 43: 183-199.
doi: 10.1016/j.firesaf.2006.07.002

[18] Jiang J, Li G Q. Disproportionate collapse of 3D steel-framed structures exposed to various compartment fires. Journal of Constructional Steel Research, 2017, 138: 594-607.
doi: 10.1016/j.jcsr.2017.08.007

[19] Jiang J, Jiang L, Kotsovinos P, Zhang J, Usmani A, Mckenna F, Li G Q. OpenSees software architecture for the analysis of structures in fire. Journal of Computing in Civil Engineering, 2015, 29(1): 04014030.
doi: 10.1061/(ASCE)CP.1943-5487.0000305

[20] Jiang S, Zhu S, Guo X, Chen C, Li Z. Safety monitoring system of steel truss structures in fire. Journal of Constructional Steel Research, 2020, 172: 106216.
doi: 10.1016/j.jcsr.2020.106216

[21] Ye Z, Hsu S C, Wei H H. Real-time prediction of structural fire responses: A finite element-based machine-learning approach. Automation in Construction, 2022, 136: 104165.
doi: 10.1016/j.autcon.2022.104165

[22] Li G Q, Ji W, Feng C, Wang Y, Lou G. Experimental and numerical study on collapse modes of single-span steel portal frames under fire. Engineering Structures, 2021, 245: 112968.
doi: /10.1016/j.engstruct.2021.112968

[23] Naser M. Z., Kodur V, Thai H T, Hawileh R, Abdalla J, Degtyarev V V. StructuresNet and FireNet: Benchmarking databases and machine learning algorithms and structural and fire engineering domains. Journal of Building Engineering, 2021, 44: 102977.
doi: 10.1016/j.jobe.2021.102977

[24] Fang H, Lo S. M, Zhang Y, Shen Y. Development of a machine-learning approach for identifying the stages of fire development in residential room fire. Fire Safety Journal, 2021, 126: 103469.
doi: 10.1016/j.firesaf.2021.103469.

[25] Mashhadimoslem H, Ghaemi A, Palacios A. Analysis of deep learning neural network combined with experiments to develop predictive models for a propane vertical jet fire. Heliyon, 2020, 6: e05511.
doi: 10.1016/j.heliyon.2020.e05511.

[26] Wang Z, Zhang T, Wu X, Huang X. Predicting transient building fire based on external smoke images and deep learning. Journal of Building Engineering, 2022, 47: 103823.
doi: 10.1016/j.jobe.2021.103823

[27] Kou L, Wang X, Guo X, Zhu J, Zhang H. Deep learning based inverse model for building fire source location and intensity estimation. Fire Safety Journal, 2021, 121: 103310.
doi: 10.1016/j.firesaf.2021.103310

[28] Raissi M, Perdikaris P, Karniadakis G E. Physics-informed neural networks: A deep learning framework for solving forward and inverse problems involving nonlinear partial differential equations. Journal of Computational Physics, 2019, 378: 686-707.
doi: 10.1016/j.jcp.2018.10.045

[29] Samaniego E, Anitescu C, Goswami S, Nguyen-Thanh V M, Guo H, Hamdia K, Zhuang X, Rabczuk T. An energy approach to the solution of partial differential equations in computational mechanics via machine learning: Concepts, implementation and applications. Computer Methods in Applied Mechanics and Engineering, 2020, 362: 112790.
doi: 10.1016/j.cma.2019.112790

[30] Rao C, Sun H, Liu Y. Physics-informed deep learning for incompressible laminar flows. Theoretical and Applied Mechanics Letters, 2020, 10(3): 207-212.
doi: 10.1016/j.taml.2020.01.039

[31] Freitag S, Graf W, Kaliske M, Sickert J U. Prediction of time-dependent structural behavior with recurrent network for fuzzy data. Computers and Structures, 2011, 89: 1971-1981.
doi: 10.1016/j.compstruc.2011.05.013

[32] Zhu H, Wang X, Chen X, Zhang L. Similarity search and performance prediction of shield tunnels in operation through time series data mining. Automation in Construction, 2020, 114: 103178.
doi: org/10.1016/j.autcon.2020.103178

[33] Zhang R, Chen Z, Chen S, Zheng J, Büyüköztürk O, Sun H. Deep long short-term memory networks for nonlinear structural seismic response prediction. Computers and Structures, 2019, 220: 55-68.
doi: 10.1016/j.compstruc.2019.05.006

[34] Xu Z, Chen J, Shen J, Xiang M. Recursive long short-term memory network for predicting nonlinear structural seismic response. Engineering Structures, 2022, 250(1): 113406.

doi: 10.1016/j.engstruct.2021.113406

[35] Zhang T, Wang Z, Wong H Y, Tam W C, Huang X. Real-time forecast of compartment fire and flashover based on deep learning. Fire Safety Journal, 2022, 130: 103579.
doi: 10.1016/j.firesaf.2022.103579

[36] Wu X, Zhang X, Huang X, Xiao F, Usmani A. A real-time forecast of tunnel fire based on numerical database and artificial intelligence. Building Simulation, 2022, 15: 511-524.
doi: 10.1007/s12273-021-0775-x.

[37] Flah M, Nueez I, Chaabene W B, Nehdi M L. Machine learning algorithms in Civil Structural Health Monitoring: A Systematic Review. Archives of Computational Methods in Engineering, 2021, 28: 2621-2643.
doi: 10.1007/s11831-020-09471-9

[38] Hasni H, Jiao P, Alavi A H, Lajnef N, Masri S F. Structural health monitoring of steel frames using a network of self-powered strain and acceleration sensors: A numerical study. Automation in Construction, 2018, 85: 334-357.
doi: 10.1016/j.autcon.2017.10.022

[39] Brownjohn J M W. Structural health monitoring of civil infrastructure. Philosophical Transactions of The Royal Society, 2007: 365: 589-622.
doi: 10.1098/rsta.2006.1925

[40] Dung D, Nguyen V K. Deep ReLU neural networks in high-dimensional approximation. Neural Networks, 2021, 142: 619-635.
doi: 10.1016/j.neunet.2021.07.027

[41] Wei Y, Duan Q, Yuan R, Yan X, Yang Y. Dropout neuronal unit with tunable probability based on NbOx stochastic memristor for efficient suppression of overfitting. Microelectronic Engineering, 2022, 259: 111778.
doi: 10.1016/j.mee.2022.111778

[42] Vijayalakshmi K, Vijayakumar K, Nandhakumar K. Prediction of virtual energy storage capacity of the air-conditioner using a stochastic gradient descent based artificial neural network. Electric Power Systems Research, 2022, 208: 107879.
doi: 10.1016/j.epsr.2022.107879

[43] Kouzehgar M, Tamilselvam Y K, Heredia M V, Elara M R. Self-reconfigurable façade-cleaning robot equipped with deep-learning-based crack detection based on convolutional neural networks. Automation in Construction, 2019, 108: 102959.
doi: 10.1016/j.autcon.2019.102959

[44] Xu D, Zhang S, Zhang H, Mandic D P. Convergence of the RMSProp deep learning method with penalty for nonconvex optimization. Neural Networks, 2021, 139: 17-23.

doi: 10.1016/j.neunet.2021.02.011
[45] Kingma D P, Ba J. Adam: A method for stochastic optimization. arXiv preprint arXiv:1412.6980, 2014.
doi: 10.48550/arXiv.1412.6980
[46] Chang Z, Zhang Y, Chen W. Electricity price prediction based on hybrid model of adam optimized LSTM neural network and wavelet transform. Energy, 2019, 187: 115804.
doi: 10.1016/j.energy.2019.07.134
[47] 02SG518-1, Design of Light Steel Portal Frames. Beijing: China Building Standard Design and Research Institute, 2002. (in Chinese)
[48] Rahman M, Xu Y. Behavior of steel portal frames in fire: comparison of implicit and explicit dynamic finite element methods. International Journal of Structural Stability and Dynamics, 2013, 13(4): 1250058.
doi: 10.1142/S0219455412500587
[49] Wong S Y, The Structural Response of Industrial Portal Frame Structures in Fire. Sheffield: University of Sheffield, 2001.
[50] Eurocode 3: Design of Steel Structures-Part 1–1: General Rules and Rules for Buildings. Brussels: European Committee for Standardization, 2005.
[51] Eurocode 1: Actions on Structures. Part 1–2: General Actions - Actions on Structures Exposed to Fire. Brussels: European Committee for Standardization, 2004.
[52] GB51249-2017: Code for Fire Safety of Steel Structures in Buildings. Beijing: China Planning Press, 2017. (in Chinese)
[53] Lou G, Wang C, Jiang J, Jiang Y, Wang L, Li G Q. Fire tests on full-scale steel portal frames against progressive collapse. Journal of Constructional Steel Research, 2018, 145: 137-152.
doi: 10.1016/j.jcsr.2018.02.024
[54] Li G, Ji W, Feng C, Wang Y, Li X, Liang T, Shi X, Liu X. Collapse test of steel portal frame under fire and effective analysis of radar-based displacement measuring system. China Civil Engineering Journal, 2021, 54(9): 56-65. (in Chinese)